Draft version January 1, 2025
Typeset using LaTeX default style in AASTeX631

Parameter dependence of the power-law relationship between solar X-ray luminosity and total unsigned magnetic flux

Keiji Yoshimura,[1] Aki Takeda,[1] and Dana W. Longcope[1]

[1] *Department of Physics, Montana State University Bozeman, MT 59717, USA*

ABSTRACT

Despite the fact that the heating mechanism of the solar corona remains to be elucidated, it is widely accepted that a magnetic field plays a key role in the process. One of the approaches for addressing the heating mechanism involves conducting a statistical study of the relationship between coronal emission and magnetic field on the photosphere. Pevtsov et al. (2003) studied the relationship between the X-ray luminosity (L_X) and the total unsigned magnetic flux (Φ_m) for a wide range of data, from solar quiet region through T Tauri stars. While they reported a single power law relationship $L_X \sim \Phi_m^{1.15}$ for whole distribution, they found a broken power law in the part of the solar full disk-integrated flux, i.e., larger index ($\sim$2) for the low magnetic flux end and smaller index for high end. There are several parameters in the calculation of the X-ray luminosity and the total unsigned magnetic flux. We studied how the selections of the parameters impact on the L_X-Φ_m distribution. While most of the parameters examined in the study did not result in significant changes to the distributions, the cut-off magnetic field strength in the calculation of the total unsigned magnetic flux substantially affect on the results. We got broken power law distributions with low cutoff values, and single power law with higher values which are above the noise level of the magnetogram. This may suggest there are weak but existing magnetic field which do not contribute to the X-ray emission.

Keywords: Solar coronal heating (1989); Solar magnetic fields (1503); Solar spectral irradiance (1501)

1. INTRODUCTION

Since Grotrian (1939) and Edlén (1943) showed that the solar corona was comprised of million degree plasma, many scientists tried to elucidate the heating mechanism of the outermost atmosphere (see Klimchuk (2015), Parnell & De Moortel (2012), Reale (2010), Klimchuk (2006) for reviews). Although the details of the heating mechanism is still unclear, a prevailing consensus exists among researchers regarding the critical role of magnetic field in the process.

One of the approaches to understanding the heating mechanism is to conduct a statistical study on the relationship between coronal emission and magnetic field on the photosphere. For example, Golub et al. (1980) and Yashiro & Shibata (2001) derived power law relationship between the thermal energy of X-ray corona and total magnetic flux of solar active regions. Fisher et al. (1998) compared the relationship between the X-ray luminosity (L_X) and various magnetic variables of active regions on the Sun. They found that the total unsigned magnetic flux (Φ_m) is best correlated with L_X, which can be expressed $L_X \sim \Phi_m^{1.19}$. They also suggested that the coronal heating with Alfvén wave can produce the relationship, which was reproduced by a numerical simulation study (Shoda & Takasao 2021). Pevtsov et al. (2003) studied the relationship between L_X and Φ_m for 12 orders of magnitude, from quiet region of the Sun through T Tauri stars. They found the relationship can be expressed by a single power law $L_X \sim \Phi_m^{1.15}$ for the whole range. Toriumi & Airapetian (2022) studied the relationship of multi temperature plasma covering from the chromosphere through corona by using both solar and stellar data. They found a trend that the power law indices is smaller for low temperature range, but for all range the indices is close to unity. On the other hand, some studies using only stellar data reported larger power law indices (Vidotto et al. 2014; Kochukhov et al. 2020).

Corresponding author: Keiji Yoshimura
keiji.yoshimura@montana.edu

The calculation of X-ray luminosity and total unsigned magnetic flux is contingent upon the selection of several critical parameters. In this paper, we tested the impact of the parameter selection on the results, with a particular focus on the power law indices.

In Pevtsov et al. (2003) they reported "knee" structure for the solar full disk data set. The different power law indices in the low magnetic flux end (index ∼2) and the high end (index ∼1) creates the structure. They suggested possibility that the existence of the coronal hole may create the structure, but did not present any evidences. One of our objectives in this study is to ascertain the nature of the "knee" structure's existence, whether it is a result of natural phenomena or an artificial influence. While Pevtsov et al. (2003) used the data from the soft X-ray telescope (SXT) onboard Yohkoh satellite and the magnetograms from the National Solar Observatory/Kitt Peak (NSO/KP), we used X-ray images from Hinode/XRT and magnetograms of SDO/HMI, to make L_X and Φ_m plots for the full Sun data.

2. DATA

2.1. *Hinode/XRT*

The X-ray Telescope (XRT) (Golub et al. 2007; Kano et al. 2008) onboard Hinode satellite (Kosugi et al. 2007) is a grazing-incidence X-ray telescope with multiple analysis filters, covering 1MK to 30MK coronal plasma. The XRT routinely takes full disk solar images with multiple exposure time and with various filters as synoptic observation. One set of the multiple exposure images of each X-ray analysis filter are composited into one image to achieve larger dynamic range of X-ray intensity (Takeda et al. 2016). We use these synoptic composite data for this study. After standard calibration processes by the IDL program xrt_prep.pro, we subtracted stray light component (Takeda et al. 2016) from the data, then created composite data.

The total X-ray flux of each composite image is calculated by integrating the intensity of all pixels within a circle of radius R_X, centered on the solar disk. The parameters R_X was introduced to mitigate the contribution of over-the-limb corona to the X-ray luminosity, which is not associated with the observable magnetic field on the solar disk.

We selected every possible pairs of the X-ray fluxes of different analysis filters taken within 3 minutes, in order to apply the filter ratio method (Vaiana et al. 1973; Narukage et al. 2011). We can obtain disk-integrated plasma temperature (Te) and emission measure (EM) through the process.

The temperature response function of the XRT undergoes variation over time due to the degradation of the instrument. Most of the corrections of the effect are well calibrated and implemented in the default processing, but we added two more corrections to modify the response function, i.e., (1) the change of the fraction of the prefilter's open portion, and (2) increase of the contamination layer on the XRT analysis filters. The implementation of these extra corrections is still in the experimental phase. We assess the impact of the corrections on the result in this paper.

In order to synthesize an X-ray spectrum from the derived Te and EM, we use two different CHIANTI models (Dere et al. 1997, 2019; Del Zanna et al. 2021) versions 9.1 and 10.0 with two different abundance models: "corona" (Feldman 1992) and "hybrid" (Fludra & Schmelz 1999). We use the same model for the XRT response function calculation in the above process for consistency.

The X-ray luminosity can be calculated by integrating the spectrum over a specified wavelength range (Wx). We started with the wavelength range which Pevtsov et al. (2003) used in their study (2.8-36.6Å) and tested other ranges to assess the impact of the selection of Wx.

We selected the XRT data taken with Al-Mesh, Al-Poly, and Thin-Be filters for this study, since they are all used in the synoptic observation for a long time covering a whole solar cycle. The temperature response function of each filter can be found in Narukage et al. (2011).

Errors in Lx due to the photon noise and systematic (non-statistical) uncertainties (Kobelski et al. 2014) are estimated to be smaller than 3% for all data sets in this study, which are small enough in log-log scale plots.

2.2. *SDO/HMI*

The Helioseismic and Magnetic Imager (HMI) onboard the Solar Dynamics Observatory (SDO) provides us with magnetograms of whole Sun (Scherrer et al. 2012; Schou et al. 2012). We use the line-of-sight magnetograms of 720 seconds cadence (Couvidat et al. 2016) for our study.

After the correction of projection effect by assuming the magnetic field is radial direction, we integrated the unsigned magnetic flux of all pixels which shows higher field strength than a cut off value (Bc) within a circle of radius Rm,

centered on the solar disk. The foreshortening effect of area corresponding to each pixel is corrected during the integration. The parameters Bc was introduced to mitigate the contribution of noises of the magnetograms.

2.3. *Lx - Φ_m plots*

We select pairs of XRT and HMI data which are taken within 1 hour difference to make a log-log scale scatter (L_X-Φ_m) plot (see figure 1 for samples of the plots). We apply linear fitting for higher and lower halves of the log-log plots separately to see the difference of the power law index of each parts, in order to see whether the distribution is expressed by single power law line or broken one. For the results showing non-trivial distinction were subjected to a further fitting process, employing a broken power law.

3. RESULTS

We listed the default values of the parameters in the table 1. In the absence of a specified value within the text, we use these default ones.

Table 1. Default values

Parameter	default value
Rx	$0.83_{\odot}$
Rm	$0.79_{\odot}$
Wx	2.8 - 36.6 A
CHIANTI version	10.0
Abundance model	Corona
XRT filter pair	Al-poly and Thin-Be
Time Average	no averaging

3.1. *Cut-off magnetic field strength (Bc)*

Figure 1 shows how the cut-off magnetic field strength (Bc) changes the results. We can reproduce the "knee" structure (Figure 1 (a) and (b)) with zero or smaller Bc. The plots become increasingly straight as the Bc value increases (figure 1 (c) and (d)). Then the plots bend the other way for higher Bc (Figure 1 (e) and (f)).

The *Bc* values which result in a single power law distribution are 40 to 50G in this case. The values are considerably higher than the noise of the HMI magnetogram (∼6.3G, Liu et al. (2012)).

The power law indices are high for the smaller Bc values and low for larger Bc. And the indices are almost unity when the distribution is expressed by a single power law. All other results in this study with different parameters demonstrate the same trend.

3.2. *Integration Radius*

With Bc=45G, the distribution can be expressed by a single power law. Figure 2 shows the map of cross-correlation coefficients between $log_{10}(L_X)$ and $log_{10}\Phi_m$ with varying pairs of Rx and Rm. Clearly, the correlation is strong for the Rx $\sim$ Rm cases. More specifically, the correlation is most pronounced when slightly larger values for Rx are assigned than for Rm. This tendency is attributed to the fact that the coronal structures observed by the X-ray expand in both the horizontal and vertical directions than the associated magnetic concentration on the photosphere. Since the cross-correlation peaks at R_X=0.80$R_{\odot}$ and R_m=0.79$R_{\odot}$, these value were selected as defaults in this study.

3.3. *Integral X-ray wavelength range*

To test different integral X-ray wavelength ranges (W_X), we split the default range (2.8-36.6 Å) into three evenly and add one longer range (36.6-60.0 Å) where the XRT has sensitivity. Figure 3 shows the *Lx* - Φ_m scatter plots

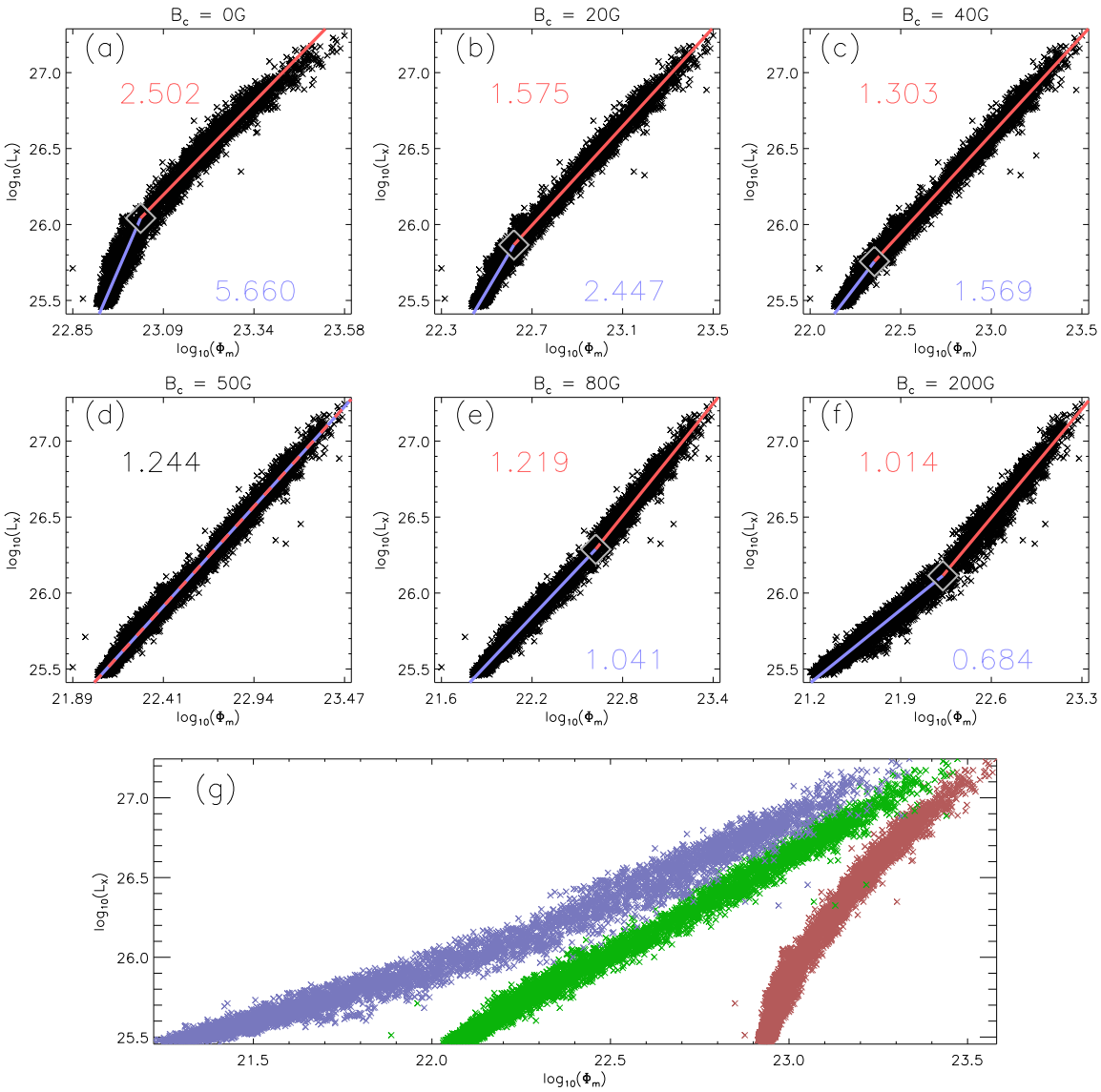

Figure 1. Log-log scale scatter plots Lx - Φ_m Wx=2.8-36.6A, XRT filter pairs Al-Poly and Thin-Be, Bc= (a)0, (b)20, (c)45, (d)55, (e)90, and (f)200G. The fitted lines are plotted in red (high end) and blue (low end) for broken power law distribution. Each power law index is displayed in red (high end), blue (low end), and black (single power law). Three results with Bc=0 (brown), 50 (green), and 200G (blue) are plotted in one graph in (g).

for different integral X-ray wavelength range. For the same Bc, the power law indices are fairly large in the short wavelength range. But they are close to unity when the distribution is expressed by a single power law. The ranges of B_c value that makes distribution expressed as single power law are different for each W_X and listed in the table 2. The values are larger in the shorter wavelength range.

3.4. *Different combination of XRT filters*

Figure 4 show the results from different XRT filter pairs, "Al-Mesh / Al-Poly" (a, b, c), "Al-Mesh / Thin-Be" (d, e, f) and "Al-Mesh / Al-Poly" (g, h, i). No major differences can be found. The ranges of Bc that makes single power law distribution are the same. The results from Al-Mesh / Thin-Be combination show more dispersion than others. This may be attributed to the difference of the temperature responses between Al-Mesh and Thin-Be filters, which is

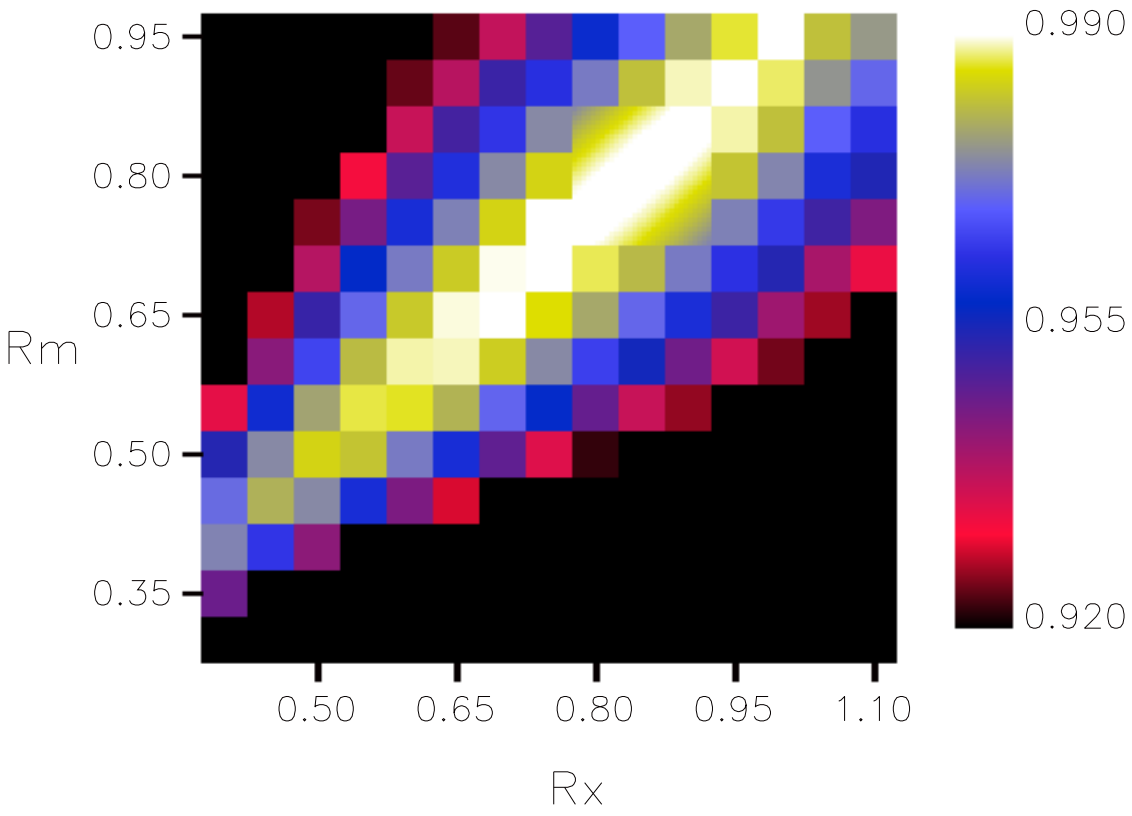

Figure 2. Map of cross-correlation coefficients between $log_{10}(L_X)$ and $log_{10}\Phi_m$ for selected Rx and Rm.

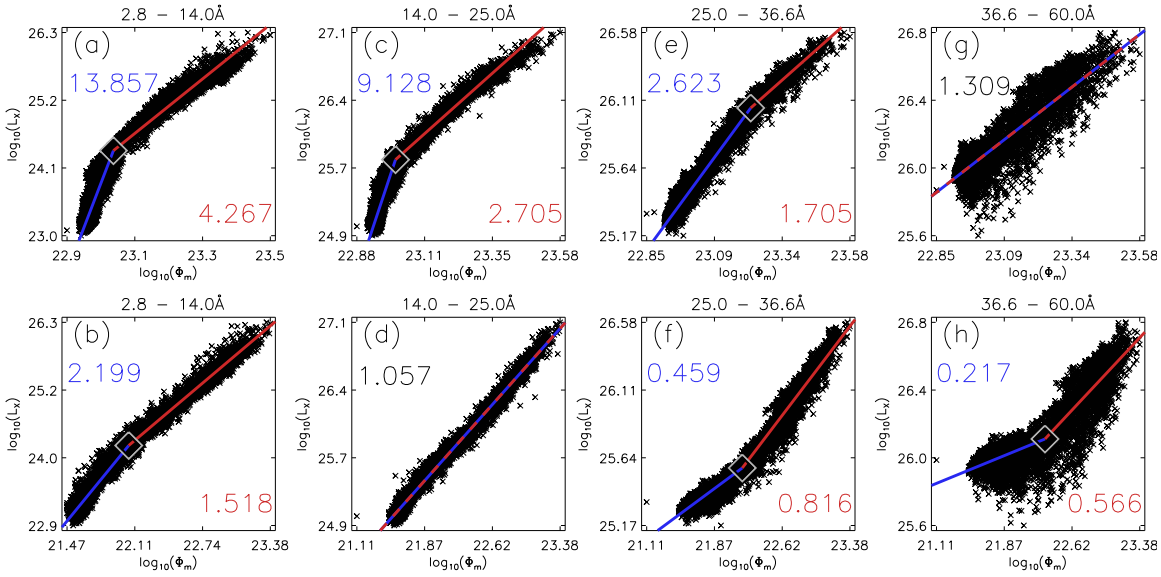

Figure 3. $L_X - \Phi_m$ distributions with different Wx, 2.8-14.0 (a, b), 14.0-25.0 (c, d), 25.0-36.6 (e, f), and 36.6-60.0Å(g, h). Bc are 0G for upper row and 150G for lower row.

the largest in all the combinations in this study. The power law indices of the combination "Al-Mesh / Al-Poly" are slightly higher than the others.

Table 2.

Wx	Bc for single power law
2.8-14.0Å	310-370G
14.0-25.0Å	130-180G
25.0-36.6Å	15- 20G
36.6-60Å	not clear due to the larger scattering

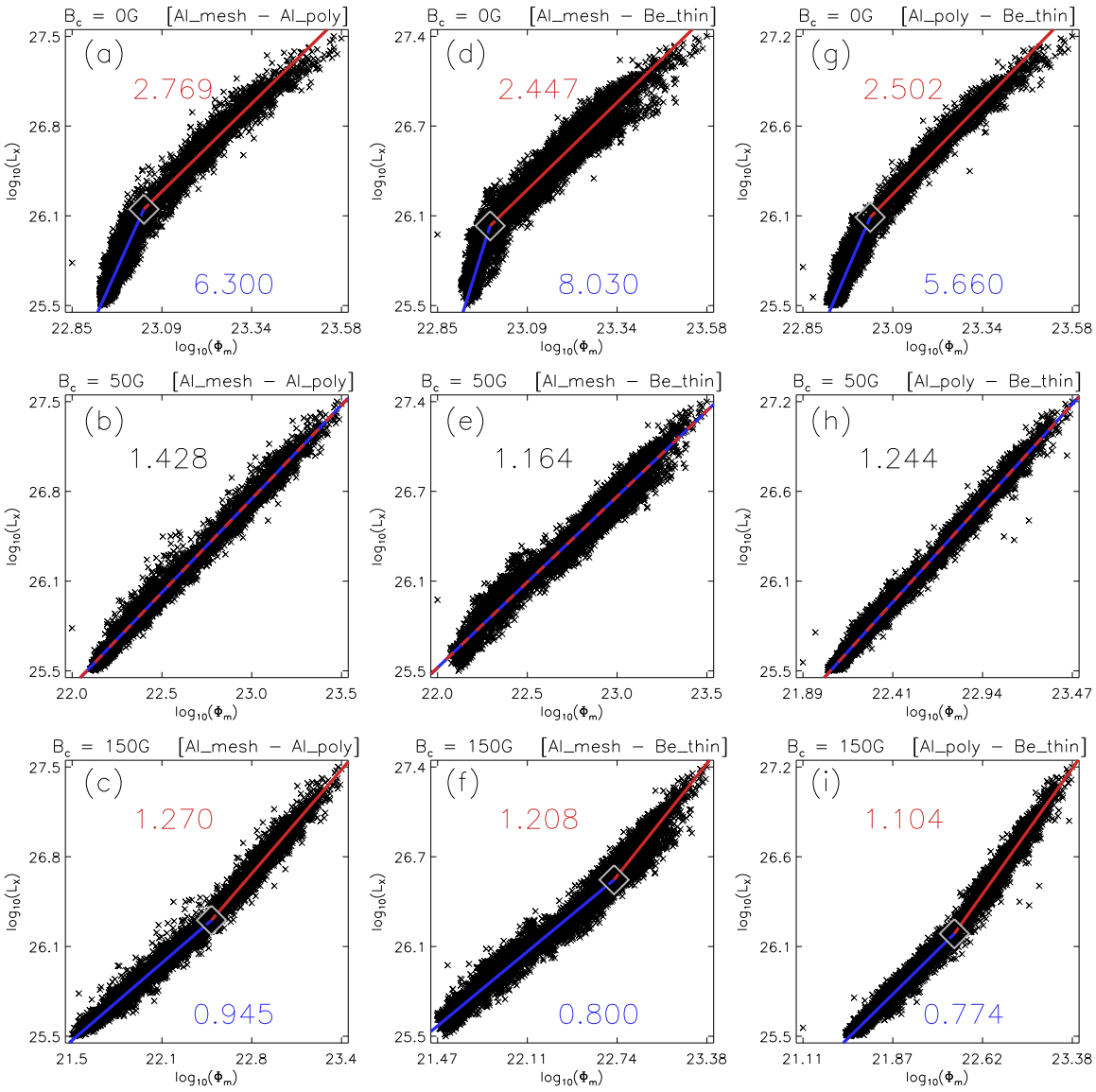

Figure 4. $L_X - \Phi_m$ distributions with different XRT filter pairs, Al-Mesh + Al-Poly (a, b, c), Al-Mesh + Thin Be (d, e, f), and Al-Poly + Thin Be (g, h, i). Bc are 0G for top row, 50G for middle, and 150G for bottom.

3.5. *CHIANTI and coronal abundance model*

The different CHIANTI versions (10.0 or 9.1) and coronal abundance models ("corona" or "hybrid") do not affect the results much. Since the luminosities calculated by CHIANTI 9.1 with "corona" abundance (Lx1) show the largest

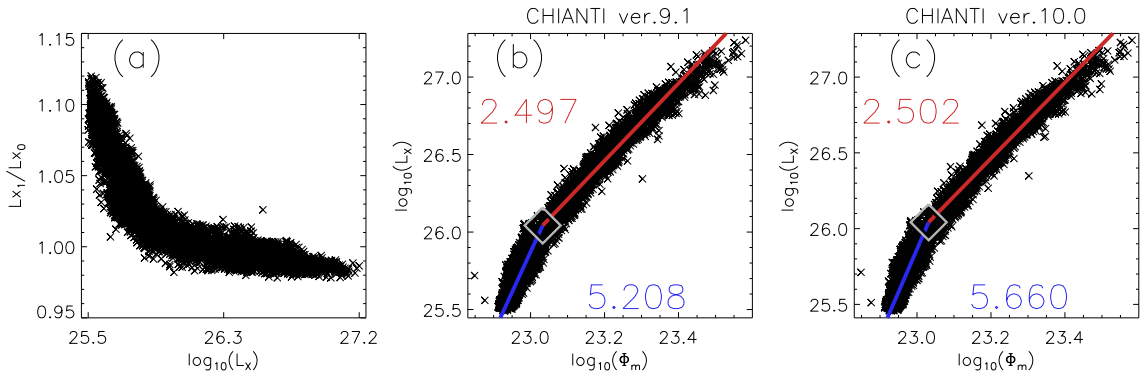

Figure 5. $L_X - \Phi_m$ distributions with different CHIANTI versions, version 9.01 (b) and 10.0 (c). The ratio of the two results is plotted in (a).

difference from the ones by 10.0 with "corona" (Lx0), we show the ratio Lx1/Lx0 in the figure 5(a) as a function of Lx0, as an example. The ratio diverges to around 1.1 at the lower luminosity end, or the solar minimum period. In other words, during the solar minimum, the X-ray luminosity calculated by CHIANTI version 9.1 is overestimated by 10% in comparison to CHIANTI version 10.0.

Even in this largest difference case, no major changes can be found in the log-log scale plots (figure 5 b and c).

3.6. *Time Average*

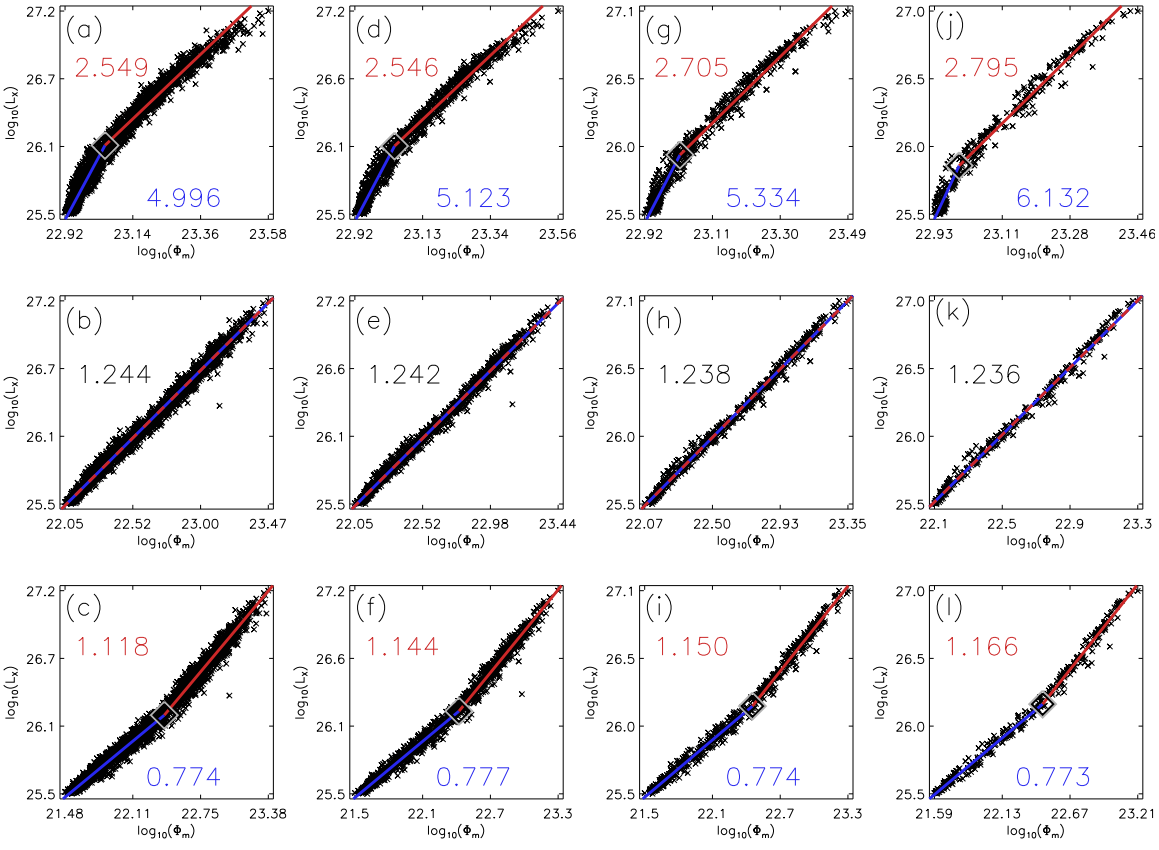

Figure 6. $L_X - \Phi_m$ distributions with different time average spans, 1 (a, b, c), 5 (d, e, f), 14 (g, h, i), and 27 days (j, k, l). Bc are 0G for the top row, 50G for the middle, and 150G for the bottom.

Pevtsov et al. (2003) used Rx=1.1R$_\odot$ for their X-ray flux calculation. So, in their case, some of the coronal structures seen in the X-ray images are not connected to the on-disk photospheric magnetic field. In order to mitigate the discrepancy, they applied solar rotation averages to magnetic and X-ray fluxes. Since we don't count the X-ray fluxes above the limb with $R_X = 0.83R_\odot$, we don't need any averaging process. But in this subsection, we show the results through different time averages just for comparison.

Figure 6 shows the results from the different time average of the data (1, 5, 14, and 27 days). The application of time averaging has the effect of reducing the dispersion to a very limited extent and does not appear to be an effective approach to reduce the noise.

3.7. *XRT extra corrections*

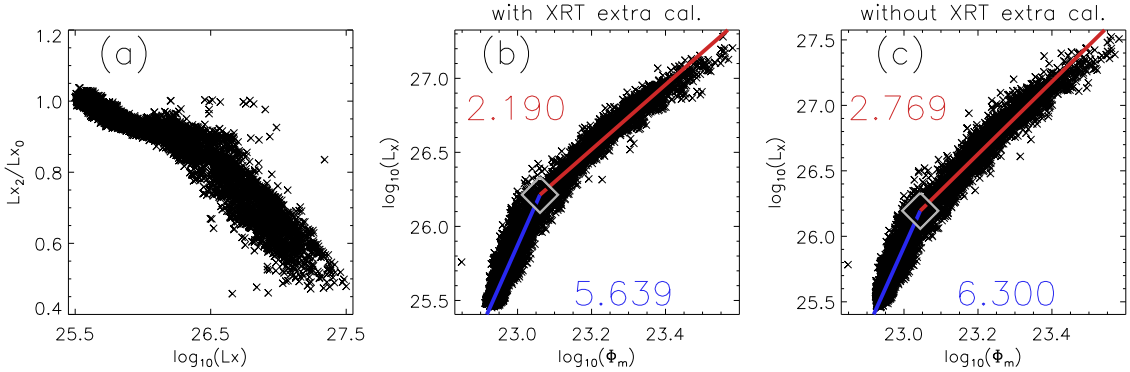

Figure 7. $L_X - \Phi_m$ distributions with (b) and without (c) the extra XRT calibration. The ratio of the two results is plotted in (a).

In order to assess the importance of the extra XRT corrections, we show the ratio of the X-ray luminosities without the corrections (Lx2) to those with the corrections (Lx0) in the figure 7 (a). Since the corrections is getting larger in time due to the degradation of the instrument, the ratio should divert from the value of 1 in the later phase. The data in this study were taken during the rising phase of the solar activity. So the plots diverts from the value of 1 in the high luminosity end.

The X-ray luminosity can be underestimated by up to 50% without the corrections. So we can tell it is important to make the corrections to calculate the X-ray luminosity in general. But the difference between the results is never large on the log-log scale plots (figure 7 (b) and (c)), so it has no major impact on the results in this study.

4. DISCUSSION

The "knee" structure reported in Pevtsov et al. (2003) can be reproduced using the more recent data set, XRT and HMI. This indicates that the structure is genuine. While most of the parameters examined in the study did not result in significant changes to the Lx-Φ_m distributions, the structure changes drastically when the Bc values is varied. In particular, the distribution is expressed by a single power law without any "knee" over a specific range of Bc which is larger than the error of the HMI magnetogram. Assuming the single power law is the "natural" distribution between Lx and Φ_m, it is necessary to ignore the weak but existing magnetic field elements when counting the total unsigned flux in order to obtain the right relationship. This may indicate that the weak magnetic field on the photosphere does not contribute to the coronal heating. It is possible that the majority of the weak magnetic field may be unable to reach the height of the corona or may lack the capacity to transport sufficient energy to the corona. Further investigation is necessary to ascertain the viability of these ideas.

Where can we find the weak magnetic field that may not contribute to coronal heating on the Sun? We show samples of quiet and active regions in figure 8. The red pixels in the top row are the places where the magnetic field strengths are stronger than the noise (3σ level, 18.9G) and weaker than 50G. They are mostly found around the strong magnetic concentrates. But some intranetwork magnetic fields are also in this range of the strength. The red area occupies only a few percentage of the total area in the samples. And the contribution to the total unsigned magnetic flux is only about 5% in the active region sample. But the total unsigned magnetic flux of the red area is nearly equivalent to that of the stronger field area in the quiet region sample.

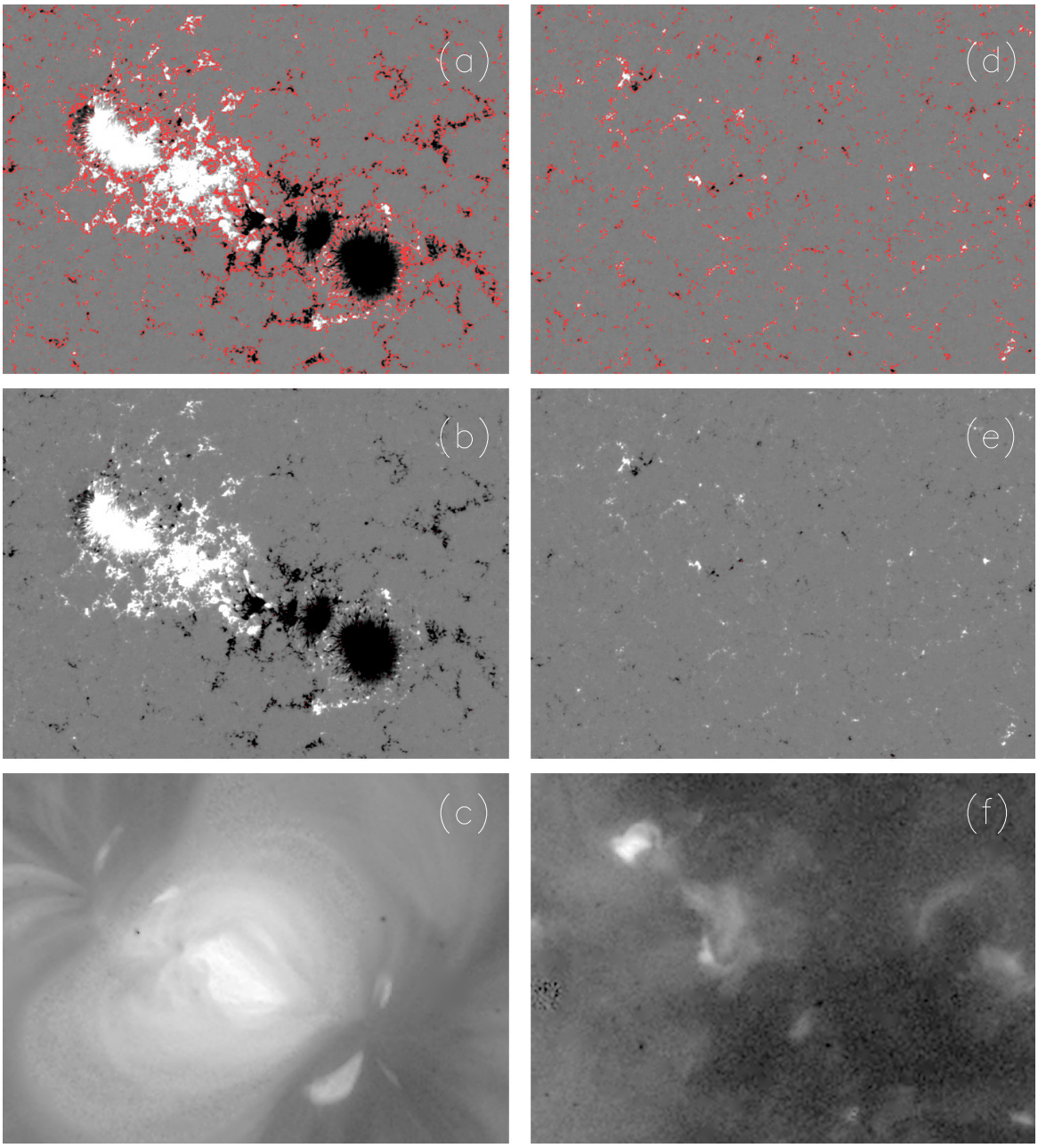

Figure 8. HMI magnetogram samples of an active region (left column) and of a quiet region including a coronal hole (right column). The XRT Al-poly images corresponding to the magnetograms are in the bottom row. The red pixels in (a) and (d) are where the magnetic field strengths are stronger than the noise (3σ level, 18.9G) and weaker than 50G.

We found smaller power law indices in longer X-ray wavelength range (Wx) for the same Bc (figure 3). Toriumi & Airapetian (2022) reported the same trend with data of much wider wavelength range. They attributed the trend to the efficiency of the plasma heating. While they measured luminosity from plasma of different temperature, we use only X-ray data with the assumption of single plasma temperature. Our results may suggest the trend can be explained by a property of emission, not by a different emission measure of different plasma temperature. In general, the emission of higher X-ray energy range is sensitive to the plasma temperature than that of lower range, which results in wider distribution of Lx. Since the distribution range of Φ_m is same for different Wx ranges, the power law indices of the shorter wavelength range tends to be higher.

It is important to note that the power law indices derived from various parameters show considerable variation. However, these indices approach unity when the distributions can be characterized by a single power law.

Hinode is a Japanese mission developed and launched by ISAS/JAXA, with NAOJ as domestic partner and NASA and STFC (UK) as international partners. It is operated by these agencies in cooperation with ESA and NSC (Norway).

REFERENCES

Couvidat, S., Schou, J., Hoeksema, J. T., et al. 2016, SoPh, 291, 1887, doi: 10.1007/s11207-016-0957-3

Del Zanna, G., Dere, K. P., Young, P. R., & Landi, E. 2021, ApJ, 909, 38, doi: 10.3847/1538-4357/abd8ce

Dere, K. P., Del Zanna, G., Young, P. R., Landi, E., & Sutherland, R. S. 2019, ApJS, 241, 22, doi: 10.3847/1538-4365/ab05cf

Dere, K. P., Landi, E., Mason, H. E., Monsignori Fossi, B. C., & Young, P. R. 1997, A&AS, 125, 149, doi: 10.1051/aas:1997368

Edlén, B. 1943, ZA, 22, 30

Feldman, U. 1992, PhyS, 46, 202, doi: 10.1088/0031-8949/46/3/002

Fisher, G. H., Longcope, D. W., Metcalf, T. R., & Pevtsov, A. A. 1998, ApJ, 508, 885, doi: 10.1086/306435

Fludra, A., & Schmelz, J. T. 1999, A&A, 348, 286

Golub, L., Maxson, C., Rosner, R., Vaiana, G. S., & Serio, S. 1980, ApJ, 238, 343, doi: 10.1086/157990

Golub, L., Deluca, E., Austin, G., et al. 2007, SoPh, 243, 63, doi: 10.1007/s11207-007-0182-1

Grotrian, W. 1939, Naturwissenschaften, 27, 214, doi: 10.1007/BF01488890

Kano, R., Sakao, T., Hara, H., et al. 2008, SoPh, 249, 263, doi: 10.1007/s11207-007-9058-7

Klimchuk, J. A. 2006, SoPh, 234, 41, doi: 10.1007/s11207-006-0055-z

—. 2015, Philosophical Transactions of the Royal Society of London Series A, 373, 20140256, doi: 10.1098/rsta.2014.0256

Kobelski, A. R., Saar, S. H., Weber, M. A., McKenzie, D. E., & Reeves, K. K. 2014, SoPh, 289, 2781, doi: 10.1007/s11207-014-0487-9

Kochukhov, O., Hackman, T., Lehtinen, J. J., & Wehrhahn, A. 2020, A&A, 635, A142, doi: 10.1051/0004-6361/201937185

Kosugi, T., Matsuzaki, K., Sakao, T., et al. 2007, SoPh, 243, 3, doi: 10.1007/s11207-007-9014-6

Liu, Y., Hoeksema, J. T., Scherrer, P. H., et al. 2012, SoPh, 279, 295, doi: 10.1007/s11207-012-9976-x

Narukage, N., Sakao, T., Kano, R., et al. 2011, SoPh, 269, 169, doi: 10.1007/s11207-010-9685-2

Parnell, C. E., & De Moortel, I. 2012, Philosophical Transactions of the Royal Society of London Series A, 370, 3217, doi: 10.1098/rsta.2012.0113

Pevtsov, A. A., Fisher, G. H., Acton, L. W., et al. 2003, ApJ, 598, 1387, doi: 10.1086/378944

Reale, F. 2010, Living Reviews in Solar Physics, 7, 5, doi: 10.12942/lrsp-2010-5

Scherrer, P. H., Schou, J., Bush, R. I., et al. 2012, SoPh, 275, 207, doi: 10.1007/s11207-011-9834-2

Schou, J., Scherrer, P. H., Bush, R. I., et al. 2012, SoPh, 275, 229, doi: 10.1007/s11207-011-9842-2

Shoda, M., & Takasao, S. 2021, A&A, 656, A111, doi: 10.1051/0004-6361/202141563

Takeda, A., Yoshimura, K., & Saar, S. H. 2016, SoPh, 291, 317, doi: 10.1007/s11207-015-0823-8

Toriumi, S., & Airapetian, V. S. 2022, ApJ, 927, 179, doi: 10.3847/1538-4357/ac5179

Vaiana, G. S., Krieger, A. S., & Timothy, A. F. 1973, SoPh, 32, 81, doi: 10.1007/BF00152731

Vidotto, A. A., Gregory, S. G., Jardine, M., et al. 2014, MNRAS, 441, 2361, doi: 10.1093/mnras/stu728

Yashiro, S., & Shibata, K. 2001, ApJL, 550, L113, doi: 10.1086/319486